24th COBEM - 2017

24th ABCM International Congress of Mechanical Engineering
December 3-8, 2017, Curitiba, PR, Brazil

COBEM-2017-0336
TRANSIENT NUMERICAL SIMULATION OF TWO-PHASE FLOW USING A COMPACT SCHEME

Bruno Resende Rodrigues
Eugênio Spanó Rosa
University of Campinas, Faculty of Mechanical Engineering, SP, Brazil
brunorodri@fem.unicamp.br

Abstract. *A simulator for transient isothermal two-phase flow using the drift-flux model is developed employing a tenth-order compact scheme to evaluate the solution numerically, using an artificial viscosity term to stabilize the solution close to discontinuities. The model is validated against two cases: a gas-liquid shock tube problem and a transient horizontal air-water flow in a pipe. In the shock tube problem, the spurious oscillations, inherent to a central order scheme, are successfully damped at the shock discontinuity due the artificial viscosity model. The model is capable of capturing the intensity and location of shock and contact discontinuities accurately. A good agreement is verified between the proposed model and experimental data in the second test case. Pressure and void fraction wave propagation velocities are calculated from the present model and are within 7% of experimental measurements.*

Keywords: *drift-flux model, transient simulation, gas-liquid flow, compact scheme, artificial viscosity*

1. INTRODUCTION

Transient flow of a gas-liquid mixture is of interest to the production of crude petroleum on the oil industry. The application of transient models often occurs at the start up or on the shut down of a line and are of interest to flow assurance analysis. Among the transient models the most popular is the one-dimensional drift-flux model because it is relatively simple and intrinsically stable. Given the complexity of coupling among the phases different strategies have been employed in simulations using this model. Romate (1998) proposed a fully numerical Roe-type solver, initially validated using the Euler equations and then used to solve a two-phase problem with the drift-flux model. A rough finite volume scheme using the drift-flux model was proposed by Faille and Heintze (1999) using a centered scheme stabilized by a "viscosity matrix". Evje and Fjelde (2002) developed hybrid solution schemes based on flux-vector splitting (FVS) and advection upwing splitting method (AUSM) schemes. The multi-stage (MUSTA) was applied to the drift-flux equations by Munkejord *et al.* (2006), showing comparable results to Roe schemes. A finite differences model was presented by Malekzadeh *et al.* (2012) using the drift-flux model to simulate severe slugging. Recently, Santim (2016) developed a Roe solver using an analytical evaluation of the Roe matrix, based on the simplifying assumption that the square of the ratio of sound propagation velocities in the gas and liquid is much smaller than unity.

This work presents a numerical model to simulate transient two-phase flow using the drift-flux model, employing a finite differences high-order compact scheme to capture shocks. Given the centered nature of the scheme, spurious oscillations arise near discontinuities. Cook and Cabot (2004) presented a non-linear artificial viscosity to stabilize the solution near shocks, which has been applied to the Euler Equations (Cook and Cabot, 2005; Fiorina and Lele, 2007; Kawai and Lele, 2008) and also multicomponent compressible flow (Kawai and Terashima, 2011). This artificial viscosity term is adapted to the drift-flux model by using mixture properties and then validated on two different test cases.

2. MATHEMATICAL FORMULATION

The drift-flux model, is presented in Eqs. (1) through (3). Equations (1) and (2) correspond to the mass conservation equations of the liquid and gas phases respectively and Eq. (3) is the mixture momentum conservation equation. Flow is assumed to the be one dimensional and isothermal, the liquid phase is assumed to be incompressible and no interphase mass transfer is considered.

$$\frac{\partial}{\partial t}[(1-\alpha)\rho_l] + \frac{\partial}{\partial x}[(1-\alpha)\rho_l v_l] = 0\,, \tag{1}$$

$$\frac{\partial}{\partial t}[\alpha\rho_g] + \frac{\partial}{\partial x}[\alpha\rho_g v_g] = 0\,, \tag{2}$$

$$\frac{\partial}{\partial t}[(1-\alpha)\rho_l v_l + \alpha\rho_g v_g] + \frac{\partial}{\partial x}[(1-\alpha)\rho_l v_l^2 + \alpha\rho_g v_g^2 + p] = s_m\,. \tag{3}$$

In Equations (1) through (3), the subscripts l and g refer to the liquid and gas phases, respectively, α is the pipe cross section void fraction, ρ_k and v_k are the density and velocity of each phase, p is the pressure and s_m is a source term for the momentum equation. This system of equations expressed in vector form is presented in Eq. (4):

$$\frac{\partial \boldsymbol{U}}{\partial t} + \frac{\partial \boldsymbol{F}}{\partial x} = \boldsymbol{S}\,, \tag{4}$$

where

$$\boldsymbol{U} = \begin{bmatrix} u_1 \\ u_2 \\ u_3 \end{bmatrix} = \begin{bmatrix} (1-\alpha)\rho_l \\ \alpha\rho_g \\ (1-\alpha)\rho_l v_l + \alpha\rho_g v_g \end{bmatrix}\,,\ \boldsymbol{F} = \begin{bmatrix} f_1 \\ f_2 \\ f_3 \end{bmatrix} = \begin{bmatrix} (1-\alpha)\rho_l v_l \\ \alpha\rho_g v_g \\ (1-\alpha)\rho_l v_l^2 + \alpha\rho_g v_g^2 + p \end{bmatrix} \quad \text{and} \quad \boldsymbol{S} = \begin{bmatrix} s_1 \\ s_2 \\ s_3 \end{bmatrix} = \begin{bmatrix} 0 \\ 0 \\ s_m \end{bmatrix}\,. \tag{5}$$

For horizontal flow, the source momentum momentum term s_m represents viscous friction inside the duct. It may be modeled as:

$$s_m = f\frac{\rho_m j_m |j_m|}{2D}\,, \tag{6}$$

where D is the pipe diameter. The mixture velocity j_m is defined in Eq. (7) in terms of the gas and liquid superficial velocities, j_g and j_l:

$$\begin{aligned} j_m &= j_g + j_l\,, \\ j_g &= \alpha v_g\,, \\ j_l &= (1-\alpha)v_l\,. \end{aligned} \tag{7}$$

The mixture density ρ_m is defined below:

$$\rho_m = \alpha\rho_g + (1-\alpha)\rho_l\,, \tag{8}$$

and the friction factor f is a function of the two-phase Reynolds number:

$$Re_m = \frac{\rho_m j_m D}{\mu_m}\,. \tag{9}$$

The mixture viscosity is defined in Eq. (10) below (Beattie and Whalley, 1982):

$$\mu_m = (1.0-\alpha)\mu_l(1.0+2.5\alpha) + \alpha\mu_g\,. \tag{10}$$

For laminar flow, the friction factor f is simply:

$$f = \frac{64}{Re_m}\,, \tag{11}$$

while for turbulent flows, the implicit Colebrook-White correlation is used:

$$\frac{1}{\sqrt{f}} = -2.0 \log\left(\frac{\epsilon/D}{3.7} + \frac{2.51}{Re_m\sqrt{f}}\right) \tag{12}$$

The density of the gas phase can be expressed in terms to the pressure p and sound velocity c_g, as given by the thermodynamic relation shown in Eq. (13). Due to the isothermal flow hypothesis, c_g is assumed to be constant.

$$\rho_g = \frac{p}{c_g^2} \,. \tag{13}$$

The system of equations given by Eq. (4) has 4 unknowns (α, p, v_l and v_g), but only 3 equations. The kinematic relation proposed by Zuber and Findlay (1965), shown in Eq. (14), provides an additional equation to close the system:

$$v_g = C_0 j_m + v_d \,, \tag{14}$$

where the distribution parameter C_0 and drift velocity v_d depend on the flow pattern and the fluid transport properties.

2.1 Numerical Model

The system of non-linear Partial Differential Equations (PDEs) presented in Eq. (4) was solved numerically. The first step in the solution is applying a spatial discretization to the $\frac{\partial \boldsymbol{F}}{\partial x}$ term, reducing the problem to a system of Ordinary Differential Equations (ODEs). The Finite Differences Method was used to achieve this, using a tenth-order compact scheme presented in Eq. (15) to approximate the spatial derivatives:

$$\beta g'_{i-2} + \gamma g'_{i-1} + g'_i + \gamma g'_{i+1} + \beta g'_{i+2} = c\frac{g_{i+3} - g_{i-3}}{6\Delta x} + b\frac{g_{i+2} - g_{i-2}}{4\Delta x} + a\frac{g_{i+i} - g_{i-i}}{2\Delta x} \,. \tag{15}$$

In this Equation, g is the function whose spacial derivative g' is to be calculated at the i-th node. In the present work, g can represent the components f_1, f_2 or f_3 of the flux vector $\boldsymbol{F}$ defined in Eq. 5. The coefficients γ, β, a, b and c required to achieve tenth order of accuracy (Lele, 1992) are shown in Eq. (16):

$$\gamma = \frac{1}{2} \,, \qquad \beta = \frac{1}{20} \,, \qquad a = \frac{1}{20} \qquad b = \frac{101}{150} \,, \qquad c = \frac{1}{100} \,. \tag{16}$$

An approximation $\delta_x \boldsymbol{F}$ of the spatial derivative $\frac{\partial \boldsymbol{F}}{\partial x}$ is obtained applying Eq. (15) to the three components of $\boldsymbol{F}$. With this approximation know, Eq. (4) can be rewritten as shown in Eq. (17):

$$\frac{\partial \boldsymbol{U}}{\partial t} = -\delta_x \boldsymbol{F} + \boldsymbol{S} = G(\boldsymbol{U}) \,. \tag{17}$$

This form of the Equation can then be integrated in time using a standard fourth order Runge-Kutta method (Lomax *et al.*, 2003) shown in Eq. (18), where Δt is the time step and h is the function being integrated in time. In the present work, h can stand for the components u_1, u_2 and u_3 of the conserved variables vector $\boldsymbol{U}$ defined in Eq. (5). Note that each sub-step is calculated only after all components of $\boldsymbol{U}$ have been evaluated for the current step in the Runge-Kutta method.

$$\begin{aligned}
\hat{h}_{n+1/2} &= h_n + \tfrac{1}{2}\Delta t G(h) \\
\tilde{h}_{n+1/2} &= h_n + \tfrac{1}{2}\Delta t G(\hat{h}_{n+1/2}) \\
\bar{h}_{n+1} &= h_n + \Delta t G(\tilde{h}_{n+1/2}) \\
h_{n+1} &= h_n + \tfrac{1}{6}\Delta t [G(h_n) + 2G(\hat{h}_{n+1/2}) + 2G(\tilde{h}_{n+1/2}) + G(\bar{h}_{n+1})]
\end{aligned} \tag{18}$$

2.2 Artificial Viscosity

When discontinuities are present in the solution, such as those from a shock wave, the compact scheme shown in Eq. (15) presents spurious oscillations and the solution might become unstable. To avoid this issue, an artificial viscous stress term τ_* is introduced into the flux vector $\boldsymbol{F}^*$, as shown in Eq. (19) below:

$$\boldsymbol{F}^* = \begin{bmatrix} f_1 \\ f_2 \\ f_3 \end{bmatrix} = \begin{bmatrix} (1-\alpha)\rho_l v_l \\ \alpha \rho_g v_g \\ (1-\alpha)\rho_l v_l^2 + \alpha \rho_g v_g^2 + p - \tau_* \end{bmatrix} . \tag{19}$$

The definition of τ_* is based on the one presented by Cook and Cabot (2004) for the Euler equations. Here, it is defined in terms of the mixture superficial velocity j_m and mixture density ρ_m, as shown in Eqs. (20) and (21):

$$\tau_* = \mu_* \frac{\partial j_m}{\partial x} , \tag{20}$$

$$\mu_* = C_\mu \rho_m (\Delta x)^{r+1} \overline{\left| \frac{\partial^r j_m}{\partial x^r} \right|} , \tag{21}$$

where μ_* is the artificial viscosity, Δx is the grid spacing, r is the order of derivative chosen and C_μ is a calibration constant. In the present work, $r = 4$ was chosen (Fiorina and Lele, 2007) and $C_\mu = 2.5$ was chosen after calibrating the computational model. The fourth derivative was evaluated as shown in Eq. (22), where $v_{m,i}^{(iv)}$ denotes the fourth derivative at the i-th point, and the operator $\overline{|v_{m,i}^{(iv)}|}$ corresponds to a Gaussian filter (Cook and Cabot, 2004), shown in Eq. (23), applied to the absolute value of $v_{m,i}^{(iv)}$.

$$\begin{aligned} \frac{7}{26} v_{m,i-1}^{(iv)} + v_{m,i}^{(iv)} + \frac{7}{26} v_{m,i-1}^{(iv)} \;=\; & \frac{1}{78(\Delta x)^4} (v_{m,i+3} - 9v_{m,i+1} + 16v_i - 9v_{m,i-1} + v_{m,i-3}) + \\ & + \frac{7}{26(\Delta x)^4} (v_{m,i+2} - 4v_{m,i+1} + 6v_i - 4v_{m,i-1} + v_{m,i-2}) , \end{aligned} \tag{22}$$

$$\begin{aligned} \overline{|v_{m,i}^{(iv)}|} = \; & \frac{3565}{10368} |v_{m,i}^{(iv)}| + \frac{3091}{12960} (|v_{m,i+1}^{(iv)}| + |v_{m,i-1}^{(iv)}|) + \frac{1997}{2592} (|v_{m,i+2}^{(iv)}| + |v_{m,i-2}^{(iv)}|) + \\ & + \frac{149}{12960} (|v_{m,i+3}^{(iv)}| + |v_{m,i-3}^{(iv)}|) + \frac{107}{103680} (|v_{m,i+4}^{(iv)}| + |v_{m,i-4}^{(iv)}|) . \end{aligned} \tag{23}$$

With τ_* properly defined, the modified flux vector $\boldsymbol{F}^*$ can be evaluated. The system of equations to be solved is then given by Eq. (24):

$$\frac{\partial \boldsymbol{U}}{\partial t} + \frac{\partial \boldsymbol{F}^*}{\partial x} = \boldsymbol{S} , \tag{24}$$

where $\boldsymbol{U}$ and $\boldsymbol{S}$ are given in Eq. (5) and $\boldsymbol{F}^*$ is defined in Eq. (19). The methodology discussed previously in this section is then used to solve this equation system. An eighth-order compact filter (Cook and Cabot, 2005) presented in Eq. (25) is applied to each component of the conserved variables vector $\boldsymbol{U}$ after each sub-step of the fourth-order Runge-Kutta method to ensure numerical stability:

$$\begin{aligned} & \beta \hat{h}_{i-2} + \gamma \hat{h}_{i-1} + \hat{h}_i + \gamma \hat{h}_{i+1} + \beta \hat{h}_{i+2} = \\ & a h_i + \frac{b}{2}(h_{i+1} + h_{i-1}) + \frac{c}{2}(h_{i+2} + h_{i-2}) + + \frac{d}{2}(h_{i+3} + h_{i-3}) + \frac{e}{2}(h_{i+4} + h_{i-4}) , \end{aligned} \tag{25}$$

where $\hat{h}$ is the filtered value of h. Here, h represents the components u_1, u_2 or u_3 of $\boldsymbol{U}$ defined in Eq. (5). The coefficients γ, β, a, b, c, d and e used in this filter are defined in Eq. (26).

$$\begin{aligned} &\gamma = 0.66624\,, \qquad \beta = 0.16688\,, \qquad a = 0.99965\,, \qquad \frac{b}{2} = 0.66652\,, \\ &\frac{c}{2} = 0.16674\,, \qquad \frac{d}{2} = 4 \times 10^{-5}\,, \qquad \frac{e}{2} = -5 \times 10^{-6}\,. \end{aligned} \tag{26}$$

3. RESULTS AND DISCUSSION

Two different test cases were employed to verify the proposed numerical method. The first case is a two-phase shock tube problem presented by Faille and Heintze (1999). It is a purely numerical case use for validation of the present method. The second case investigates transient two-phase slug flow in a horizontal duct, including a source term for friction. The numerical results are then compared against experimental data from Dalla Maria (2016) for validation.

3.1 Two-Phase Shock Tube

A two-phase shock tube problem presented by Faille and Heintze (1999) was used to test the proposed method. The shock tube has a length $L = 90\ m$, with the discontinuity situated at $x_d = 45\ m$. Initial conditions are defined for $x < 45\ m$ and $x \geq 45\ m$ as presented in Eq. (27). In addition to them, the drift-flux model parameters were adopted as $C_0 = 1.07$ and $v_d = \sqrt{0.5194}\ m/s$, the liquid phase density was $\rho_l = 1000\ kg/m^3$ and gas phase sound velocity was $c_g = 300\ m/s$. The simulation was run on two different grids, with $N_x = 200$ or $N_x = 500$ discrete points. No source terms are considered in this problem, that is, $s_m = 0$ in Eq. (5).

$x < 45\,m$	$x > 45\,m$
$\alpha_L = 0.55$	$\alpha_R = 0.55$
$v_{g,L} = 29.6\,m/s$	$v_{g,R} = 2.511\,m/s$
$p_L = 524204.07\,Pa$	$p_R = 804299.96\,Pa$

(27)

Knowing α, v_g and p from the initial conditions, the remaining flow variables can be calculated. The gas phase density ρ_g is evaluated from Eq. (13) and its superficial velocity j_g is calculated from Eq. (7). The superficial velocity j_l of the liquid phase is then obtained from Eq. (14) and the velocity v_l is calculated using Eq. (7).

Figure 1 shows the results obtained at $t = 0.6\,s$. There are two shocks, at approximately $x = 20\,m$ and $x = 85\,m$, and a contact discontinuity at approximately $x = 51\ m$. Both shocks and the contact discontinuity are well captured by the presented scheme, even on the coarser grid. A good agreement is found between the present solution and the one obtained by Faille and Heintze (1999), presented in the Figure as a reference solution. It is interesting to note that the artificial stress term τ_*, shown in Fig. 1d, has two peaks at the positions of the shocks and is essentially zero everywhere else in the domain, dampening the oscillations that would happen near the shocks without affecting the solution elsewhere. Spurious oscillations appear at the contact discontinuity, as can be seen in the graphs for void fraction and gas superficial velocity in Figs. 1a and 1b, caused by startup errors due to the sharp initial condition imposed. This effect is not present in the pressure graph in Fig. 1c, as it stays constant through the contact discontinuity.

3.1.1 Smooth Initial Condition

The shock tube problem was also solved using a smooth initial condition, based on a procedure by Kawai and Terashima (2011) for the Euler equations. For a generic primitive variable q, where, for this problem, $q = \alpha$, p or v_g, its initial value is given by Eq. (28). The smooth function f_{sv} present in Eq. (28) is defined in Eq. (29).

$$q = q_L(1 - f_{sv}) + q_R f_{sv}\,. \tag{28}$$

$$f_{sv} = \frac{1 + \mathrm{erf}\left(\dfrac{x - x_d}{C_\epsilon \Delta x}\right)}{2}\,. \tag{29}$$

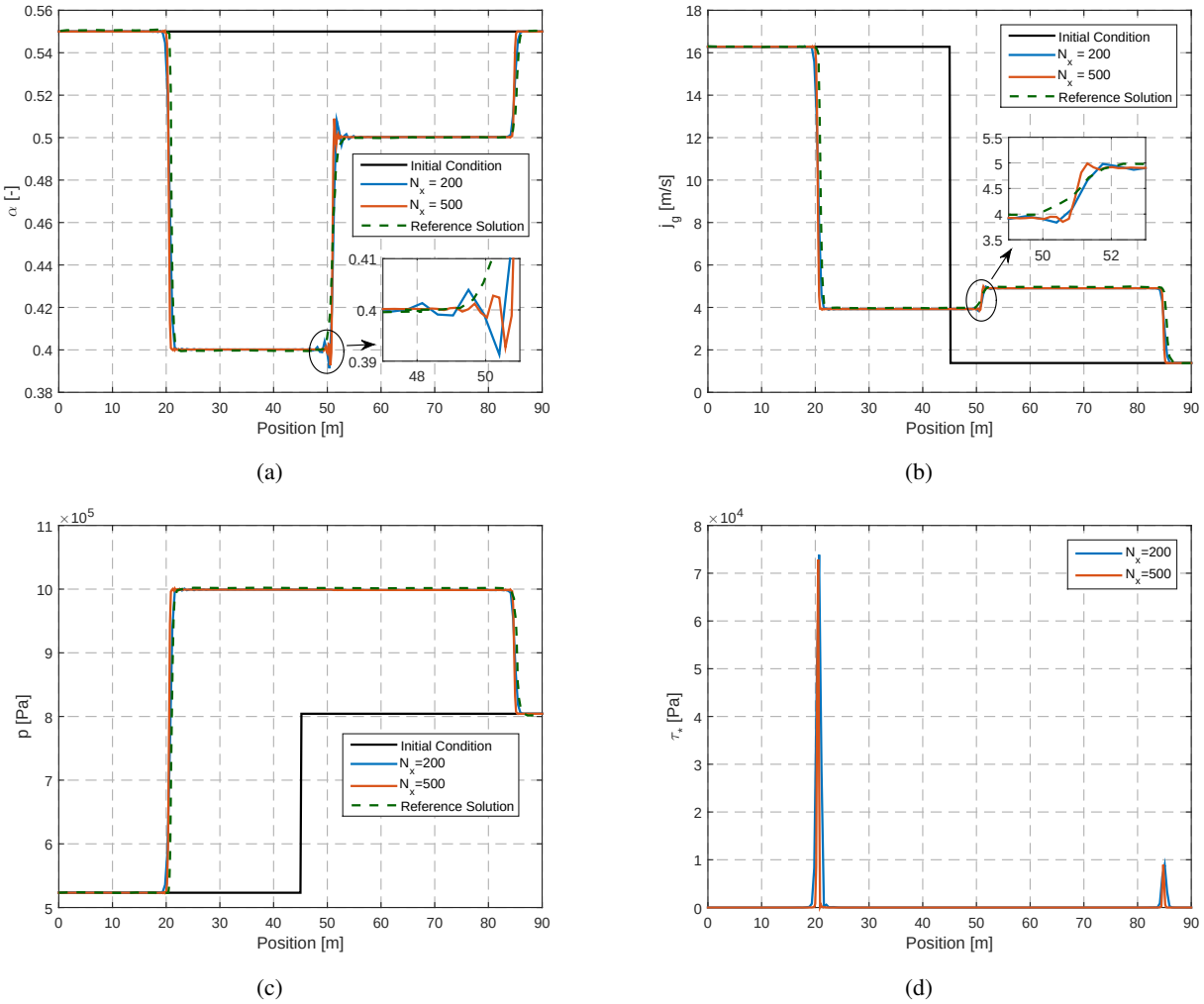

Figure 1: Numerical results for the shock tube problem at $t = 0.6\ s$. (a) void fraction; (b) gas superficial velocity; (c) pressure; (d) artificial stress

The calibration constant $C_\epsilon = 2.0$ was used for this problem and $x_d = 45\ m$ is the initial position of the discontinuity at the middle of the shock tube. The shock tube was solved with the initial values of α, p and v_g evaluated according to Eq. (28), with their left (q_L) and right (q_R) values given by Eq. (27). The remaining variables, v_l and ρ_g, are then obtained using the procedure explained previously for the sharp initial condition.

The results for void fraction, gas superficial velocity, pressure and artificial stress obtained with the smooth initial condition are presented in Fig. 2, accompanied by the results of Faille and Heintze (1999) as a reference solution. Once again, a good agreement is verified between the obtained and reference solutions. The oscillations in the void fraction profile, Fig. 2a, are considerable smaller when compared to those previously shown in Figure 1a for the sharp initial condition. The gas superficial velocity profile, Fig. 2b also shows considerably less oscillations with this smooth initial condition when compared to Fig. 1b and the pressure profile shown in Fig. 2c is practically unchanged from Fig.1c. The artificial stress peaks present in Fig. 2d coincide with the position of shocks in the other graphs.

3.2 Transient Horizontal Air-Water Slug Flow

This case is based on experimental data by Dalla Maria (2016) for transient air-water slug flow in a horizontal pipe. The test duct has a diameter D of $0.026\ m$ and a length L of $26.237\ m$. Four data acquisition stations were placed along the line in order to measure void fraction and pressure. Their positions are shown in Table 1. The ambient pressure and temperature during the experiments were, respectively, $p_0 = 93.7\ kPa$ and $T_0 = 25\ ^\circ C$. The liquid phase had a density $\rho_l = 998.0\ kg/m^3$ and viscosity $\mu_l = 8.94 \cdot 10^{-4}\ Pa.s$ and the gas phase viscosity was $\mu_g = 1.84 \cdot 10^{-5}\ Pa.s$.

The simulation was performed using $N_x = 201$ discrete points as the computational domain. The C_0 and v_d parame-

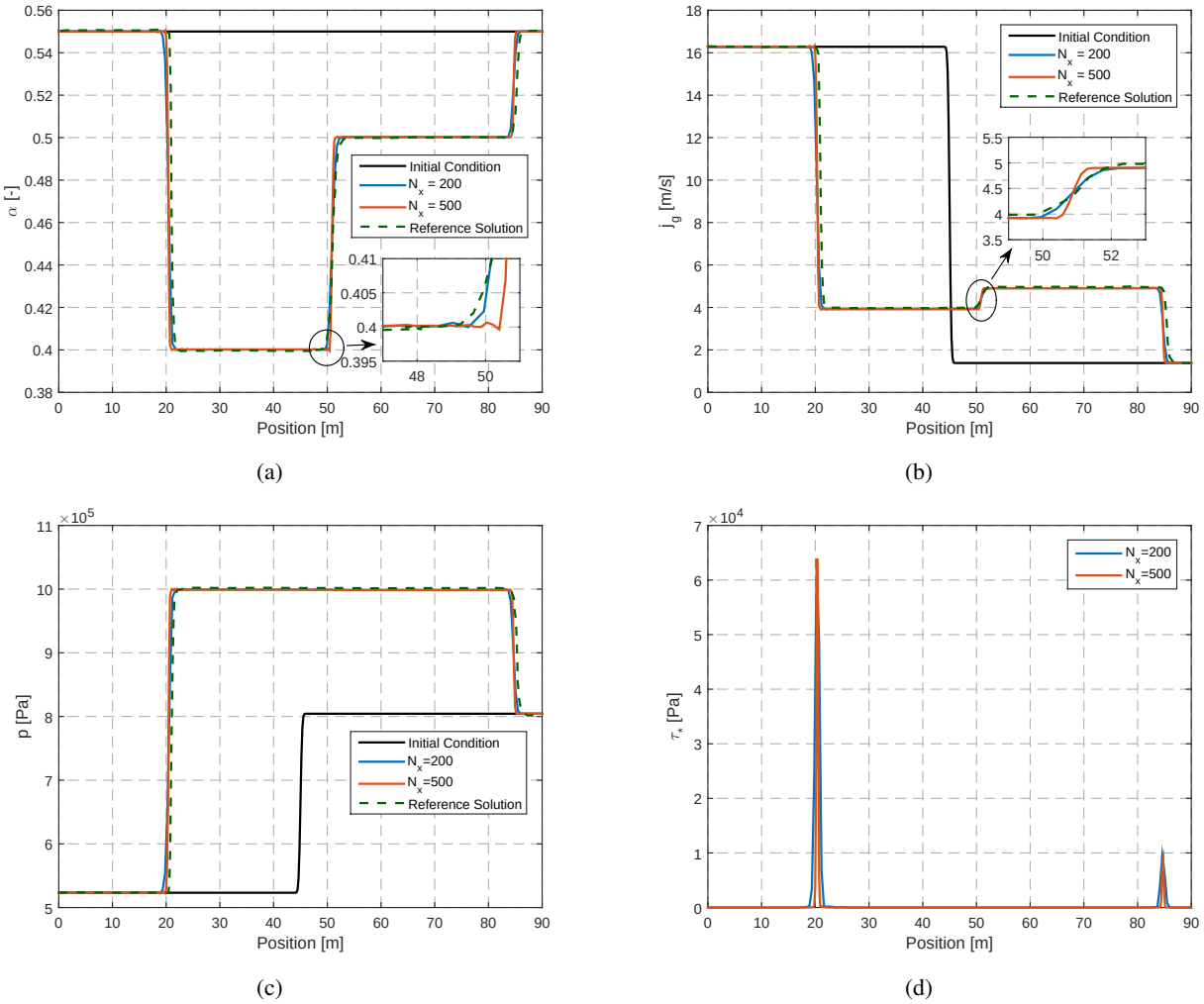

Figure 2: Numerical results for the shock tube problem at $t = 0.6\ s$, considering a smooth initial condition. (a) void fraction; (b) gas superficial velocity; (c) pressure; (d) artificial stress

ters present in Eq. (14) were evaluated using the correlations shown in Eqs. (30) and (31) (Choi *et al.*, 2012):

$$C_0 = \frac{2}{1+(\frac{Re_m}{1000})^2} + \frac{1.2 - 0.2\sqrt{\frac{\rho_g}{\rho_l}}(1-e^{-18\alpha})}{1+(\frac{1000}{Re_m})^2}, \tag{30}$$

$$v_d = A\cos\theta + B\left[\frac{g\sigma(\rho_l-\rho_g)}{\rho_l^2}\right]^{1/4}\sin(\theta), \tag{31}$$

where $A = 0.0246$, $B = 1.606$, θ is the angle in relation to the horizontal plane (θ = 0 in the present case), g is the gravitational acceleration and Re_m is the mixture Reynolds number, defined in Eq. (9). Frictional losses were considered as a source term s_m, defined in Eq. (6), during this simulation.

At the initial instant, the inlet superficial velocities, j_g and j_l are constant and equal to $0.5960\ m/s$ and $0.6040\ m/s$ respectively. At the instant $t = 30.5\ s$, a valve closes and the gas superficial velocity is reduced smoothly until $t = 37.0\ s$. A fit of the gas velocity change during the time interval of $30.5\ s$ until 37.0 is given by Eq. (32). For times greater than $37.0\ s$ the gas gas superficial velocity is maintained at a constant value $j_g = 0.2986\ m/s$ while the liquid superficial velocity is kept at the same value, $j_l = 0.6040\ m/s$.

$$\begin{aligned} j_g[cm/s] \quad = \quad & -0.0051843137t^6 + 1.0796188771t^5 - 93.5778450501t^4 + 4321.1427927699t^3 \\ & -112113.5148721740t^2 + 1549567.9581513000t - 8912995.3204702300 \end{aligned} \tag{32}$$

Table 1: Measurement Station positions, downstream from the inlet

Station	Position (m)
S1	3.98
S2	7.98
S3	14.31
S4	22.61

The void fraction and pressure time histories at four axial pipe locations are compared in Figure 3. The Figure compares the numerical data against the experimental data from Dalla Maria (2016). The numerical solutions for the void fraction and pressure capture the experimental data trend, but overestimate the void fraction by up to 13%, towards the end of the simulation, and underestimate the pressure by up to $2\,\%$ when compared to the experimental data, as shown in Figs. 3a and 3b respectively. The numerical solution is dependent on the friction factor as well as from the drift correlation; the use of distinct closure equations for these might improve the result, but an exhaustive search was not conducted. Another aspect of the numerical solution is the time delay of void fraction front. The delay is due the fact that the experimental data has a slug initiation process while the numerical solution starts from the inlet, ($x = 0$) as a developed slug flow. The pressure drops rapidly and then slowly rises until approximately $t = 56.0\ s$ in all four measurement stations and then a new steady state is achieved.

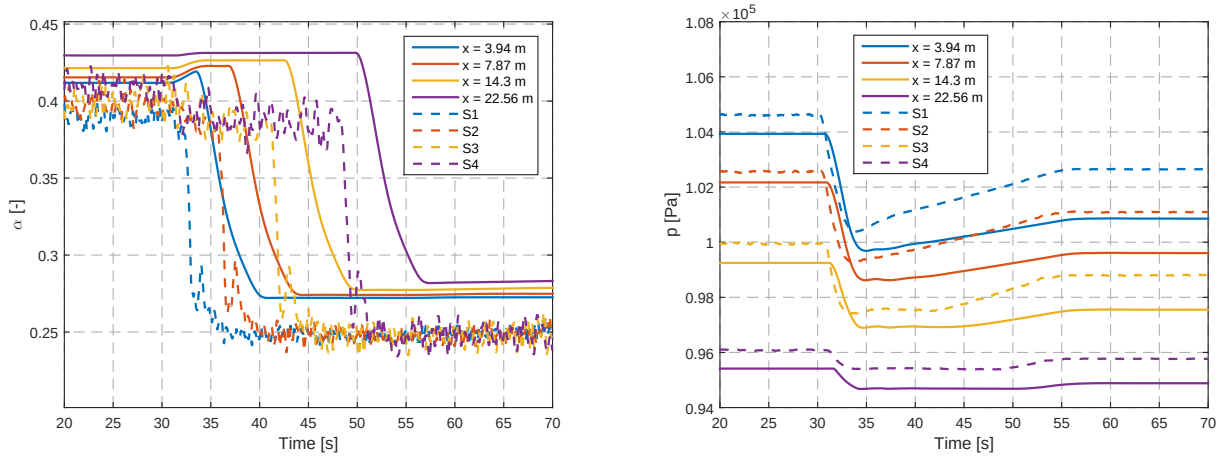

(a) (b)

Figure 3: Numerical results for horizontal two-phase flow in a pipe compared against experimental data by Dalla Maria (2016). (a) void fraction; (b) pressure. Numerical results are indicated by continuous lines and experimental results are indicated by dashed lines.

The wave velocities of the void fraction and pressure were also evaluated and are presented in Tables 2 and 3 respectively, along with experimental values by Dalla Maria (2016). Each propagation velocity is evaluated between a pair of stations as shown in Eq. (33):

$$c_k = \frac{(\Delta x)_{st}}{\Delta t}\ , \tag{33}$$

where c_k is the propagation velocity of the void fraction or pressure wave, $(\Delta x)_{st}$ is the distance between two different measurement stations, given by Table 1 and Δt is the time the wave takes to travel between the two stations. The numerical propagation velocities shown in Tables 2, and 3 are in good agreement with the experimental data. The largest relative errors occur when the wave propagation speeds are measured between Stations S1 and S2, with a 5.54% relative error being obtained in the void fraction wave velocity and a 6.64% error in the pressure wave velocity.

Table 2: Propagation velocity of the void fraction wave. Experimental values by Dalla Maria (2016).

Stations	Wave velocity (m/s)		Relative Error (%)
	Experimental	Numerical	
S1-S2	1.17	1.11	5.54%
S1-S3	1.16	1.11	3.91%
S1-S4	1.16	1.12	3.40%
S2-S3	1.16	1.12	3.40%
S2-S4	1.16	1.12	3.04%
S3-S4	1.16	1.13	2.76%

Table 3: Propagation velocity of the pressure wave. Experimental values by Dalla Maria (2016).

Stations	Wave velocity (m/s)		Relative Error (%)
	Experimental	Numerical	
S1-S2	24.1	22.5	6.64%
S1-S3	22.8	22.7	0.33%
S1-S4	22.0	22.6	2.95%
S2-S3	23.1	22.9	1.02%
S2-S4	22.8	22.7	0.49%
S3-S4	23.5	22.6	4.03%

4. CONCLUSIONS

A tenth-order finite differences compact scheme was assembled to solve transient two-phase flow problems using the drift-flux model. The compact scheme is validated using two test cases, the first being a two-phase shock tube problem. To combat spurious oscillations, an artificial viscosity model, proportional to the fourth derivative of the mixture superficial velocity, is implemented on the numerical scheme. This artificial viscosity achieves high values at the shocks, stabilizing the solution around them, but is essentially zero in the rest of the domain, preserving the solution away from shocks. However, due to the sharp initial condition and nature of the numerical method, spurious oscillations are still present close to the contact discontinuity in the solution. The shock tube was also solved with a smooth initial condition, which considerably reduced these oscillations.

The second validation case studied transient horizontal air-water slug flow in a horizontal pipe. The simulation results showed good agreement with experimental data. The numerical solution overestimated the void fraction profile and underestimated pressure values, but the qualitative behavior of the solution was well-captured. The propagation velocities of void fraction and pressure waves were also calculated and were within 7% of experimental measurements. The next developments on the model concern the implementation of the energy equation extending the model's capability to simulate non-isothermal transient flow.

5. ACKNOWLEDGEMENTS

The authors acknowledge CAPES for the financial support. The authors would like to thank Prof. Dr. William R. Wolf for fruitful discussions about compact schemes and usage of the artificial viscosity.

6. REFERENCES

Beattie, D.R.H. and Whalley, P.B., 1982. "A simple two-phase frictional pressure drop calculation method". *Int. J. Multiph. Flow*, Vol. 8, No. 1, pp. 83–87.

Choi, J., Pereyra, E., Sarica, C., Park, C. and Kang, J.M., 2012. "An Efficient Drift-Flux Closure Relationship to Estimate Liquid Holdups of Gas-Liquid Two-Phase Flow in Pipes". *Energies*, Vol. 5, pp. 5294–5306.

Cook, A.W. and Cabot, W.H., 2004. "A high-wavenumber viscosity for high-resolution numerical methods". *J. Comput. Phys.*, Vol. 195, pp. 594–601. doi:10.1016/j.jcp.2003.10.012.

Cook, A.W. and Cabot, W.H., 2005. "Hyperviscosity for shock-turbulence interactions". *J. Comput. Phys.*, Vol. 203, pp. 379–385. doi:10.1016/j.jcp.2004.09.011.

Dalla Maria, L., 2016. *Estudo Experimental das Ondas de Fração de Vazio e Pressão em Escoamento Horizontal Transiente de Ar e Água no Padrão Intermitente*. Dissertation, Faculty of Mechanical Engineering, State University of

Campinas.

Evje, S. and Fjelde, K.K., 2002. "Hybrid Flux-Splitting Schemes for a Two-Phase Flow Model". Vol. 701, pp. 674–701. doi:10.1006/jcph.2001.6962.

Faille, I. and Heintze, E., 1999. "A rough finite volume scheme for modeling two-phase flow in a pipeline". Vol. 28, pp. 213–241.

Fiorina, B. and Lele, S.K., 2007. "An artificial nonlinear diffusivity method for supersonic reacting flows with shocks". Vol. 222, pp. 246–264. doi:10.1016/j.jcp.2006.07.020.

Kawai, S. and Lele, S.K., 2008. "Localized artificial diffusivity scheme for discontinuity capturing on curvilinear meshes". Vol. 227, pp. 9498–9526. doi:10.1016/j.jcp.2008.06.034.

Kawai, S. and Terashima, H., 2011. "A high-resolution scheme for compressible multicomponent flows with shock waves". , No. March 2010, pp. 1207–1225. doi:10.1002/fld.

Lele, S.K., 1992. "Compact Finite Difference Schemes with Spectral-like Resolution". *J. Comput. Phys.*, , No. 103, pp. 16–42. doi:10.1016/0021-9991(92)90324-R.

Lomax, H., Pulliam, T.H. and Zingg, D.W., 2003. *Fundamentals of Computational Fluid Dynamics*.

Malekzadeh, R., Belfroid, S.P.C. and Mudde, R.F., 2012. "Transient drift flux modelling of severe slugging in pipeline-riser systems". *Int. J. Multiph. Flow*, Vol. 46, pp. 32–37. ISSN 0301-9322. doi:10.1016/j.ijmultiphaseflow.2012.06.005.

Munkejord, S.T., Evje, S. and Flatten, T., 2006. "The multi-stage centred-scheme approach applied to a drift- ux two-phase ow model". , No. 0316, pp. 679–705.

Romate, J.E., 1998. "An approximate Riemann Solver for a two-phase flow model with numerically given slip relation". Vol. 27, No. 4, pp. 455–477.

Santim, C.G.d.S., 2016. *Simulação Computacional de Sistemas Gás- Líquido em Regime Transiente Empregando o Modelo de Mistura*. Ph.D. thesis, Universidade Estadual de Campinas.

Zuber, N. and Findlay, J.A., 1965. "Average Volumetric Concentration in Two-Phase Flow Systems". *J. Heat Transfer*, Vol. 87, No. 4, pp. 453–468. doi:10.1115/1.3689137.

7. RESPONSIBILITY NOTICE

The authors are the only responsible for the printed material included in this paper.